Journal of Solid State Chemistry **147,** 3–10 (1999)
Article ID jssc.1999.8078, available online at http://www.idealibrary.com on IDEAL®

Modeling Stacking Faults in the Layered Molecular-Based Magnets $AM^{II}Fe(C_2O_4)_3$ $\{M^{II} = Mn, Fe; A = Organic\ Cation\}$

Christopher J. Nuttall and Peter Day

The Royal Institution of Great Britain, 21 Albemarle Street, London, W1X 4BS, United Kingdom
E-mail: PDay@ri.ac.uk

Received July 14, 1998; in revised form October 21, 1998; accepted October 23, 1998

The influence of stacking faults in the crystal structures of molecular-based magnets $N(n\text{-}C_nH_{2n+1})_4M^{II}Fe'^{III}(C_2O_4)_3$ $\{M^{II} = Mn, Fe; n=3–5\}$ is discussed on the basis of X-ray powder diffraction profiles. Polycrystalline samples of $N(n\text{-}C_5H_{11})_4$ compounds are monophasic with orthorhombic unit cells very similar to those of $N(n\text{-}C_5H_{11})_4Mn^{II}Fe^{III}(C_2O_4)_3$ determined by single crystal data. However, polycrystalline $N(n\text{-}C_3H_7)_4$ and $N(n\text{-}C_4H_9)_4$ compounds are biphasic, containing varying contributions from *R*3*c* and *P*6(3) phases. Structures containing stacking faults were modeled by assuming random interchange between *R*3*c* and *P*6(3) stacking within the crystallites. X-ray diffraction profiles calculated from the model structures exhibit broadening similar to that seen in the experimental profiles. The presence of stacking faults explains the difficulty in obtaining macroscopic single crystals of the $N(n\text{-}C_3H_7)_4$ and $N(n\text{-}C_4H_9)_4$ compounds. © 1999 Academic Press

INTRODUCTION

The crystal structures of the bimetallic *tris*-oxalato molecular-based magnets $AM^{II}M'^{III}(C_2O_4)_3$ contain honeycomb layers (1), within each of which octahedrally coordinated M and M' alternate, connected through ambidentate oxalate ligands. The connectivity of the honeycomb layer requires adjacent *tris*-oxalate units to have alternating enantiomeric configurations, Δ and Λ, so that, within a given layer all the M have one configuration and all the M' the other. The inorganic layers are interleaved by organic cations, A, whose size controls the interlayer separation (2). A large number of compounds with this general formula have been reported by varying M, M', and A (1–4), and consequently a wide variety of magnetic ground states have been achieved, including ferro, antiferro and a range of ferrimagnets (5), though crystal structures from single crystal X-ray diffraction are available only for a limited number of examples owing to the difficulty in obtaining suitable crystals (1, 4, 6–8). Nevertheless it is clear that the layer honeycomb topology is maintained throughout the series, while the organic cation plays an important part in determining the stacking of the layers, as well as the precise local symmetry at the metal ion sites. This point is illustrated by the layer stacking sequences found within the homologous series $N(n\text{-}C_nH_{2n+1})_4M^{II}M^{III\prime}(C_2O_4)_3$ $(n = 3–5)$ for which full structures are available (Table 1). In orthorhombic $N(n\text{-}C_5H_{11})_4Mn^{II}Fe^{III}(C_2O_4)_3$ the inorganic layers stack in a two layer [a-b'] repeat structure (7) (where $'$ indicates a reversal of metal *tris*-oxalate configurations within layers). The arrangement of the metal ions in this structure is illustrated in Fig. 1. Among $N(n\text{-}C_4H_9)_4M'^{II}M^{III}(C_2O_4)_3$ compounds, two hexagonal structural refinements have been reported: those of $N(n\text{-}C_4H_9)_4Mn^{II}Cr^{III}(C_2O_4)_3$ refined in *R*3*c* (6) and $N(n\text{-}C_4H_9)_4Mn^{II}Fe^{III}(C_2O_4)_3$ refined in *P*6(3) (8). The stacking of inorganic layers in the two structures is illustrated in Fig. 2. The *R*3*c* structure has a six-layer [a-b'-c-a'-b-c'] repeat, while that in *P*6(3) is [a-b]. Finally, $N(n\text{-}C_3H_7)_4Mn^{II}Cr^{III}(C_2O_4)_3$ has also been refined in *R*3*c* with the same stacking sequence (8) as that of $N(n\text{-}C_4H_9)_4Mn^{II}Cr^{III}(C_2O_4)_3$.

The unusual magnetic properties of the series $AM^{II}Fe^{III}(C_2O_4)_3$ $\{M^{II} = Mn, Fe\}$, whose low temperature magnetization varies greatly with the organic cation A, have been studied using polycrystalline samples (2). Powder X-ray diffraction profiles of these materials show a variety of unusual effects such as peak broadening, large peak asymmetry at low angle, and sharp decreases in reflection intensities at high scattering angles, indicative of structural disorder. The degree of disorder also depends on the details of the synthetic route. In this paper we report the modeling of observed powder X-ray diffraction profiles, first by assuming the structures found by single crystal diffraction and second by assuming random sequences of two layer packing types.

EXPERIMENTAL

The compounds $(cation)M^{II}Fe^{III}(C_2O_4)_3$ were precipitated in powder form using two general methods which we label the (a) block and (b) ionic methods:

0022-4596/99 $30.00

TABLE 1
Space Groups and Unit Cell Constants of $N(n\text{-}C_nH_{2n+1})_4MM'(C_2O_4)_3$ Determined by Single Crystal X-Ray Diffraction

(Cation)	$M^{II}M'^{III}$	T (K)	Space group	Unit cell (Å)	V (Å^3)	Ref.
$N(n\text{-}C_3H_7)_4$	MnCr	RT	$R3c$	$a = 9.363$, $c = 49.207$	3736	8
$N(n\text{-}C_4H_9)_4$	MnCr	RT	$R3c$	$a = 9.414$, $c = 53.66$	4118	6
$N(n\text{-}C_4H_9)_4$	MnFe	RT	$P6(3)$	$a = 9.482$, $c = 17.827$	1388	8
$N(n\text{-}C_5H_{11})_4$	MnFe	120	C222(1)	$a = 9.707$, $b = 16.140$, $c = 19.883$	3115	7

(a) The block method: an aqueous solution of $K_3Fe(C_2O_4)_3$ (100 mM) was mixed with an equimolar quantity of M^{II} in 100 mM solution {for $M^{II} = Fe^{II}$, $Fe(SO_4)\cdot 6H_2O$, for $M^{II} = Mn^{II}$, $MnCl_2\cdot 6H_2O$}. The solution was left standing for approximately 1 h and then filtered to remove precipitated $M^{II}C_2O_4\cdot 2H_2O$. A water/methanol solution containing an equimolar quantity of the organic cation ($\sim$100 mM) was then slowly added to the filtrate during stirring. After approximately 12 h the precipitated (cation)$M^{II}Fe^{III}(C_2O_4)_3$ was filtered from the solution, dried, and stored under vacuum.

(b) The ionic method: A solution of $Fe^{III}(NO_3)_3\cdot 6H_2O$ (50 mM), M^{II} ions (50 mM) and oxalic acid {150 mM) was prepared in a (1 : 1 : 3) molar ratio (for $M^{II} = Fe^{II}$, $Fe(SO_4)\cdot 6H_2O$, with a few drops of 1 M HCl added upon Fe^{II} dissolution, for $M^{II} = Mn^{II}$, $MnCl_2\cdot 6H_2O$}. After approximately 1 h any precipitated $M^{II}C_2O_4\cdot 2H_2O$ was removed by filtration. A molar quantity of the organic cation equal to that of the metal ions was then added to the filtrate and dissolved with addition of the minimum volume of methanol. The precipitated (cation)$M^{II}Fe^{III}(C_2O_4)_3$ was filtered after 24 h, dried, and stored under vacuum.

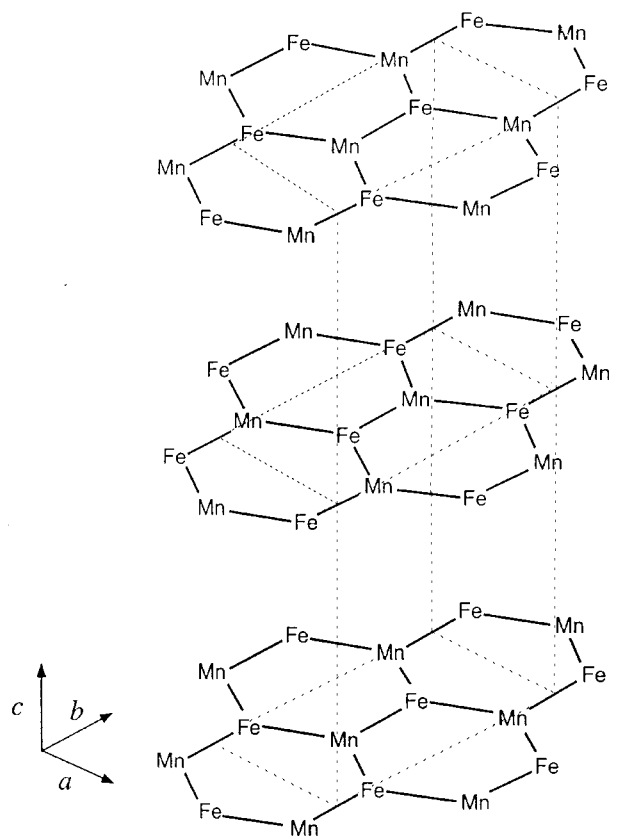

FIG. 1. The inorganic layer framework in $N(n\text{-}C_5H_{11})_4MnFe(C_2O_4)_3$.

The competing biproduct phase $M^{II}C_2O_4\cdot 2H_2O$ was initially identified in X-ray diffraction scans of the compounds, and was visible as a yellow powder in green (cation)$Fe^{II}Fe^{III}(C_2O_4)_3$ samples. The primary filtration step was necessary to remove this impurity, which re-formed when precipitation of (cation)$M^{II}Fe^{III}(C_2O_4)_3$ is extended beyond 1–2 days. The block method was the initial preparative route to the (cation)$M^{II}Fe^{III}(C_2O_4)_3$ compounds (5), but it suffers several disadvantages compared to the ionic method. Precipitation by the block method was also more rapid being practically complete in 1 h compared to several hours by the ionic route, probably because of the need to form $[Fe(C_2O_4)_3]^{3-}$ in solution. It was noticable that the slower precipitation by the ionic method also gave more crystalline products as indicated by their powder diffraction profiles.

X-ray powder profiles were collected using a Siemens D500 X-ray diffractometer set in Bragg–Brentano geometry. Samples were very lightly ground and mounted on a flat sample plate. Typically, profiles were collected as step scans over a 12-h period with a step size of 0.01° 2θ. Extending the collection times further resulted in noticeable sample discoloration and loss in diffraction intensity.

The model structures used to simulate the powder diffraction profiles were generated from the atomic positional parameters of the published crystals (6–8) by making the appropiate substitutions of the metal ions. $P6(3)$ structural models for compounds containing $N(n\text{-}C_3H_7)_4$ were generated by placing $N(n\text{-}C_3H_7)_4$ on the $N(n\text{-}C_4H_9)_4$ site of the $P6(3)$ $N(n\text{-}C_4H_9)_4MnFe(C_2O_4)_3$ structure and displacing it from the oxalate layer along c so that $N(n\text{-}C_3H_7)_4$ was displaced by the same distance as in $R3c$ $N(n\text{-}C_3H_7)_4$ $MnCr(C_2O_4)_3$.

In layered materials structural disorder frequently arises from a poor correlation between the orientation of adjacent

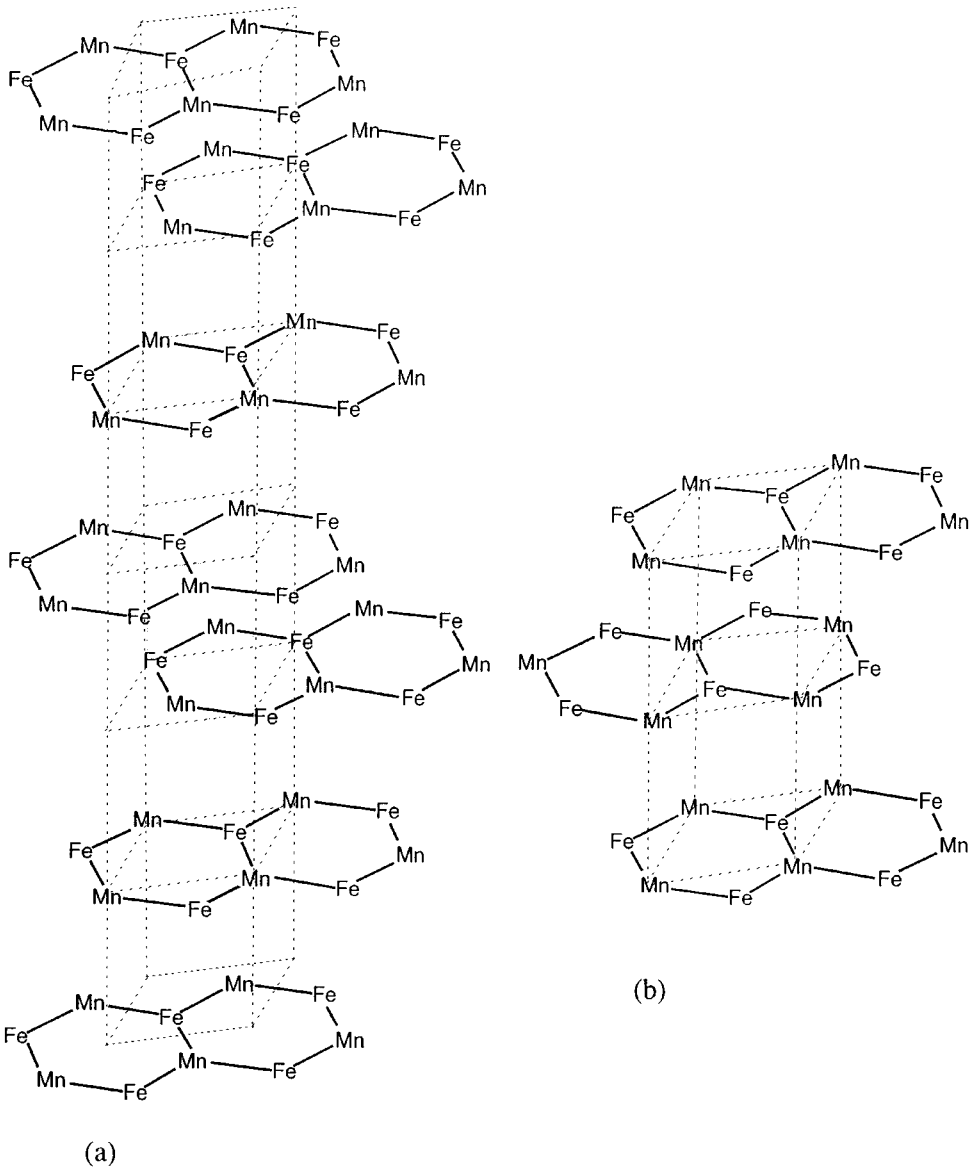

FIG. 2. The inorganic layer framework in the cation)$MM'(C_2O_4)_3$ structures: (a) *R*3*c*, (b) *P*6 (3).

layers as a result of translating the rigid planes. Two limiting cases of disorder may be identified. In one case layers stack in a random fashion with a complete loss of interplanar registry. The coherent diffraction intensity is only observed for [00*l*] reflections, [*hk*0] reflections exhibiting weak two-dimensional diffraction and [*hkl*] reflections having no coherent intensity (10). In the second case, there are a finite number of possible translational vectors between successive layers. This type of layer disorder, known as stacking faulting, results in streaks in the reciprocal lattice, giving [*hkl*] dependent broadening of peaks in the powder diffraction pattern (11). We simulated X-ray powder diffraction patterns of the $N(n\text{-}C_3H_7)_4$ compounds with both *R*3c and *P*6(3) layer stacking and also for cases where the stacking is faulted between each type, using the Diffraction Intensities in Faulted Xtals (DIFFaX) program (11,12). The crystal is defined by infinite sheets of layer unit cells stacked in sequence with defined stacking vectors ($\mathbf{R}_{ij}$) between adjacent layers. Faulting is simulated by introducing alternative layers and/or stacking vectors within a layer sequence by using stacking probabilities (α_{ij}) for each possible $\mathbf{R}_{ij}$.

RESULTS

X-ray powder diffraction profiles of $N(n\text{-}C_5H_{11})_4M^{II}Fe^{III}(C_2O_4)_3$ (M^{II} = Mn, Fe) are shown in Fig. 3 fitted to the

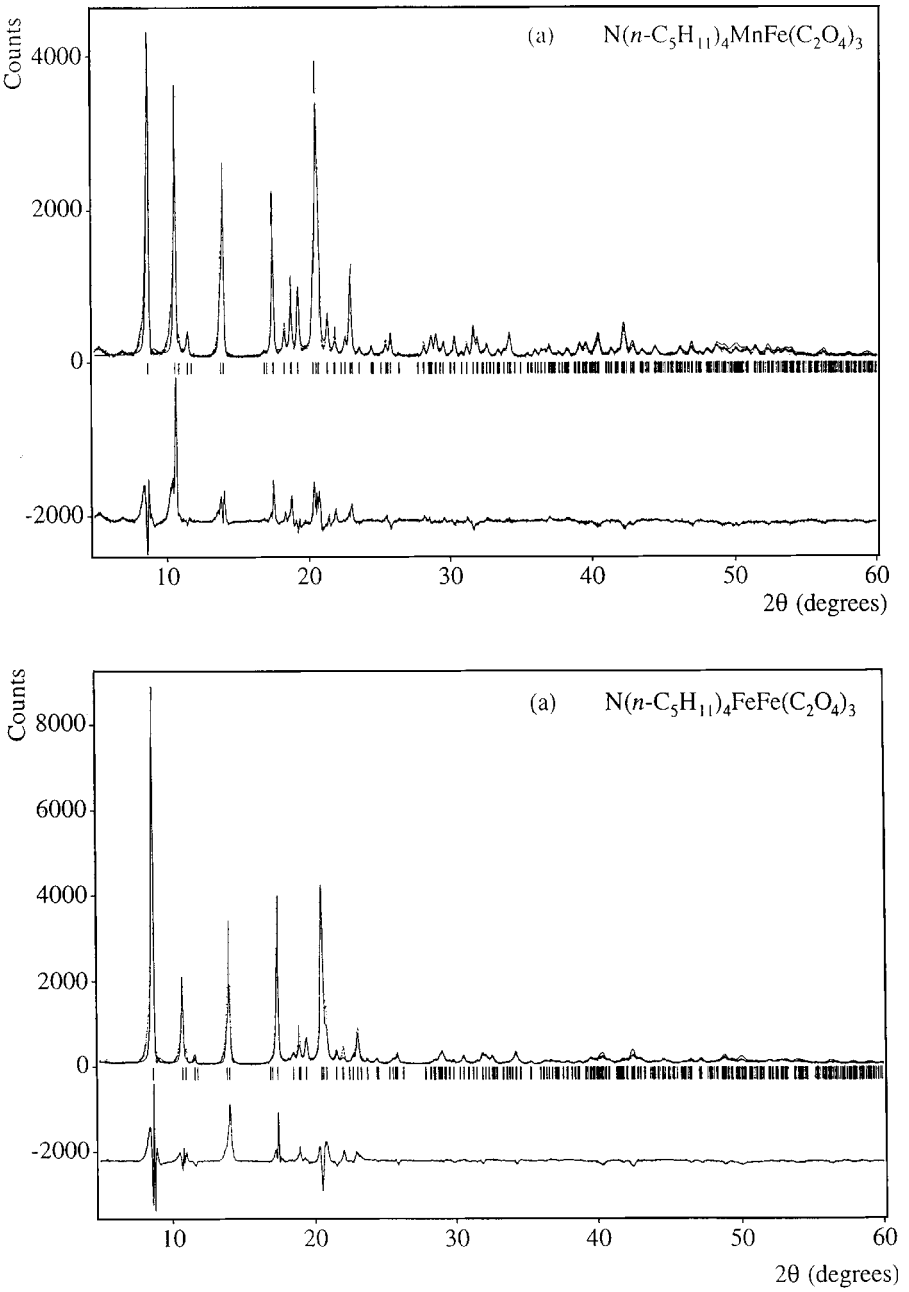

FIG. 3. $N(n\text{-}C_5H_{11})_4MnFe(C_2O_4)_3$ powder diffraction profile fitted to the single crystal $N(n\text{-}C_5H_{11})_4MnFe(C_2O_4)_3$ structural model.

structural model of $N(n\text{-}C_5H_{11})_4Mn^{II}Fe^{III}(C_2O_4)_3$, derived from the single crystal X-ray diffraction data collected at 120 K (7) refining lattice parameters and including the effects of preferred microcrystalline orientation (9). Despite the poor fit to the peak shape given by the pseudo-Voigt function with added low angle asymmetry corrections, it is clear that the powder samples are monophasic with structures very similar to the model. In an earlier paper the X-ray powder diffraction profiles of the $N(n\text{-}C_4H_9)_4$ and $N(n\text{-}C_3H_7)_4$ compounds were indexed and the unit cell constants extracted by relaxing the *R*3*c* reflection conditions (2). Fitting the structural models now available from single crystal X-ray diffraction to the powder profiles reveals that the powders are in fact biphasic, containing contributions from both *P*6(3) and *R*3*c* phases. Figure 4 shows the fits to the $N(n\text{-}C_3H_7)_4M^{II}Fe^{III}(C_2O_4)_3$ profiles. In the calculated profiles in Figure 4 the corresponding unit cells of the *P*6(3) and *R*3*c* structures have been constrained to be equal. The good

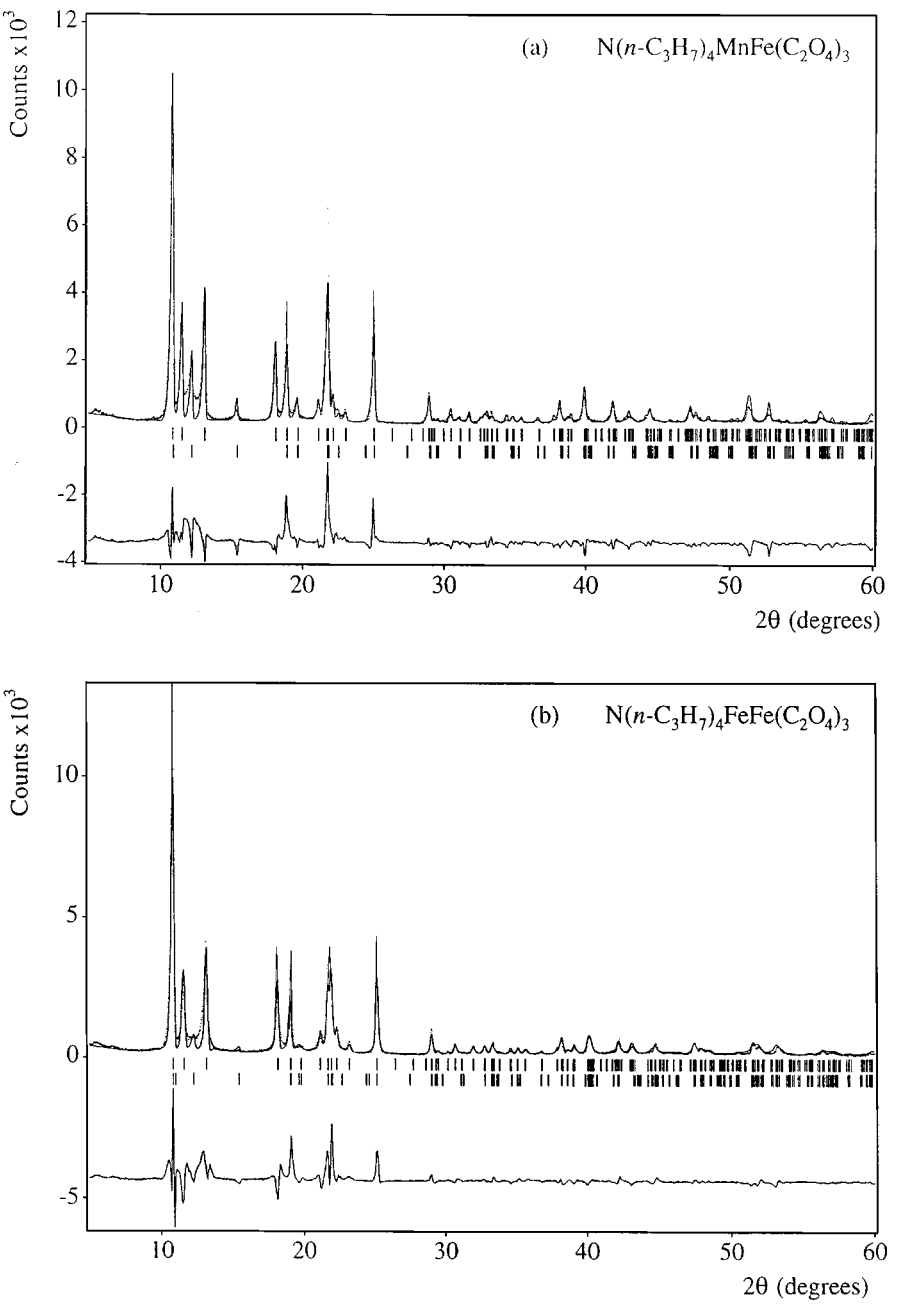

FIG. 4. Two phase fits for $N(n\text{-}C_3H_7)_4M^{II}Fe(C_2O_4)_3$; fitting to $R3c$ and $P6(3)$ structural models for (a) M^{II} = Mn, (b) M^{II} = Fe.

fit indicates that this assumption is correct, with $a(R3c) = a(P6(3)) \pm 0.01$ Å and $c(R3c) = 3 \times c(P6(3)) \pm 0.1$ Å. By inspection, the reflections attributed to the $P6(3)$ phase are broader and their line shapes have larger Lorentzian contributions compared to those from the $R3c$ phase. Given the similarity of layer stacking in the $R3c$ and $P6(3)$ structures (Fig. 2), there is a strong possibility that each powder-crystallite contains both stacking types, i.e., the compounds suffer from stacking faults.

The $R3c$ structural model was generated by dividing the cell into six-layer $P1$ unit cells $a,b = 9.416$ Å and $c = 8.18$ Å (13). The $P1$ cells of layers 1, 3, and 5 are related by the rhombohedral centring of $R3c$ while layers 2, 4, and 6 are generated from the c-glide plane in $R3c$. The full structure is described by two $P1$ layer cells stacking alternately with a six-layer repeat, as illustrated in Fig. 5, where the $\mathbf{R}_{ij}$ vectors are defined in terms of the layer unit cell. Setting the transition probabilities between each successive layer equal

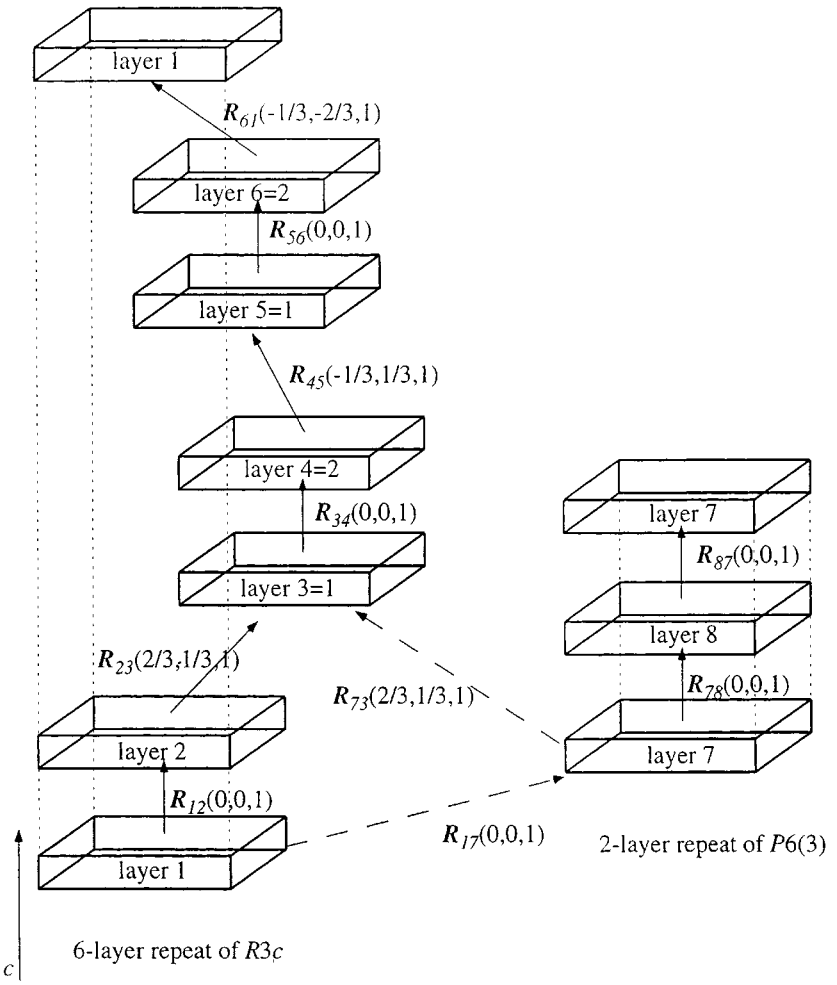

i) *R*3*c* simulation; $\alpha_{12} = \alpha_{23} = \alpha_{34} = \alpha_{45} = \alpha_{56} = \alpha_{61} = 1$, all other $\alpha_{ij} = 0$.

ii) *R*3*c* ↔ *P*6(3) stacking faulting simulation (probability of faulting n);

α_{12} = 1-n, α_{17} = n, α_{78} = 1-n, α_{73} = n,

$\alpha_{23} = \alpha_{34} = \alpha_{45} = \alpha_{56} = \alpha_{61} = \alpha_{87} = 1$, all other $\alpha_{ij} = 0$.

FIG. 5. The layer unit cells of *R*3*c* and *P*6(3) model structures and their stacking vectors.

to unity ($\alpha_{i \to i+1} = 1$) generates the diffraction profile of the *R*3*c* structure (Fig. 6a). The *P*6(3) structural model of $N(n\text{-}C_3H_7)_4MnFe(C_2O_4)_3$ was defined by two *P*1 layer unit cells, identical to the *R*3*c* ones, stacked as in Fig. 5. The calculated profile is shown in Fig. 6b.

As far as the positions of the metal ions are concerned, layer 2 in *R*3*c* suffers the same displacement as layer 1 of *P*6(3). The layers in *P*6(3), will now be referred to as 7 and 8, corresponding to 1 and 2 in *P*6(3), respectively. Faulting between the two structures can therefore be simulated by generating an eight-layer structure with nonzero stacking probabilities for the stacking vectors $\mathbf{R}_{17}$ and $\mathbf{R}_{73}$ ($\alpha_{17} = \alpha_{73} \neq 0$) (see Fig. 5).

Powder diffraction profiles of the faulted layer structure were then calculated for different faulting probabilities, $n = \alpha_{17} = \alpha_{73}$ (with $\alpha_{17} = \alpha_{73}$ the fractions of *R*3c and *P*6(3) are constrained to be equal). The calculated profiles are displayed in Figs. 6c–6g for $n = 0.01$ (1% faulting probability),

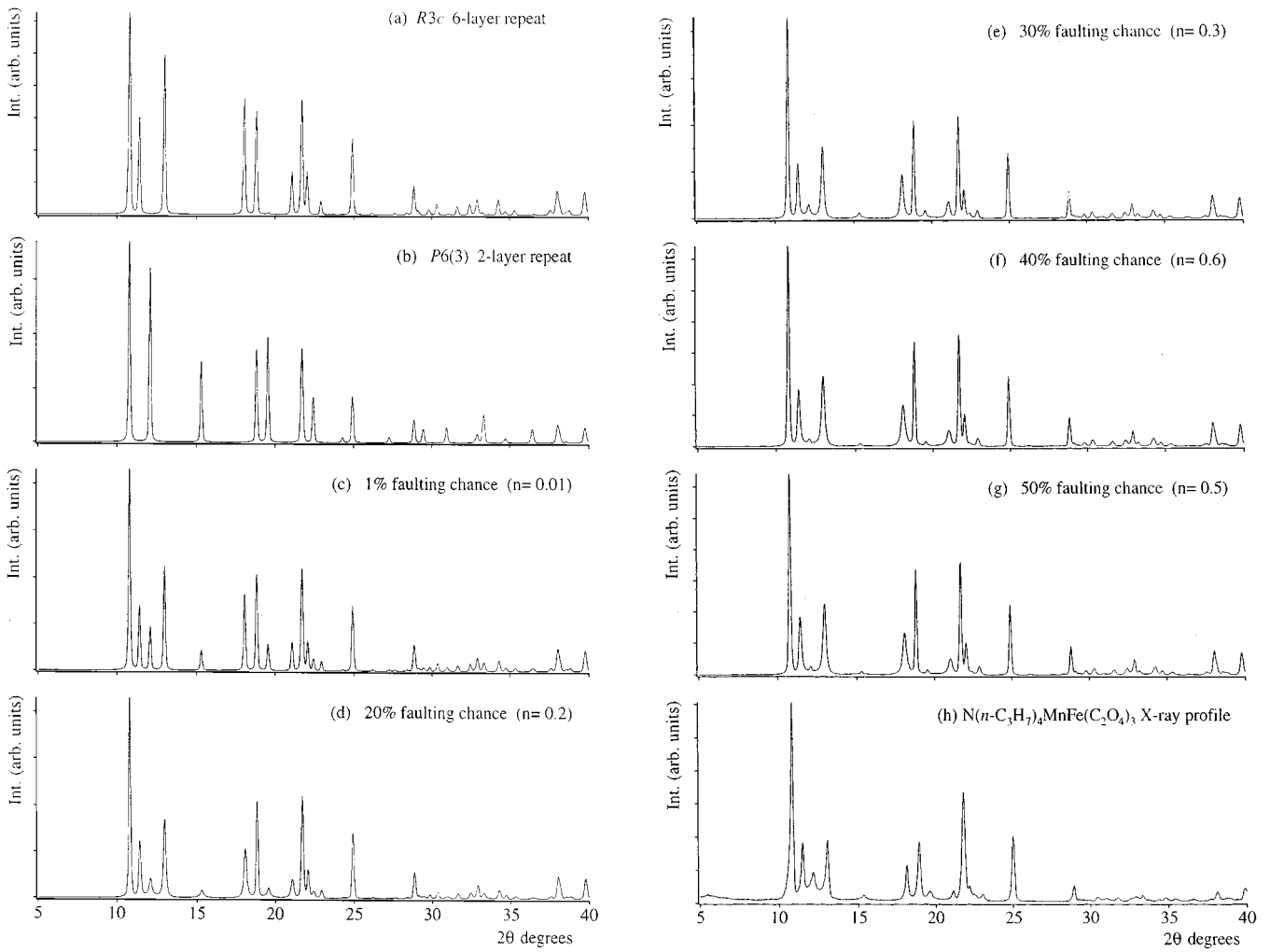

FIG. 6. Powder X-ray diffraction profiles of $N(n\text{-}C_3H_7)_4MnFe(C_2O_4)_3$: (a–f) simulated as described in the text; (g) observed.

0.2 (20%), 0.3 (30%), 0.4 (40%), and 0.5 (50%), while the measured profile of $N(n\text{-}C_3H_7)_4MnFe(C_2O_4)_3$ is displayed for comparison in Fig. 6h.

A faulting chance of 1% between *P*6(3) and *R*3*c* gives a calculated X-ray profile equivalent to the sum of *R*3*c* and *P*6(3) phases, since it corresponds to $\sim$100 *R*3*c* or *P*6(3) cells between faults ($\sim$4800 Å in the *R*3*c* structure). Higher faulting probabilities ($\geq$20%) result in an overall broadening of the reflections. Reflections originating from the *P*6(3) phase become relatively weaker with increasing faulting probability and their lineshapes exhibit large Lorentzian broadening. The same effect is also noticable in the $N(n\text{-}C_3H_7)_4MnFe(C_2O_4)_3$ experimental profile. The simulation procedure does not allow us to optimize the fit by varying the stacking probability by least squares minimization, but it is clear from Fig. 6 that the closest correspondence between observed and simulated profiles corresponds to a faulting probability of between 20 and 30%.

CONCLUSIONS

The simulated X-ray diffraction profiles of $N(n\text{-}C_3H_7)_4M^{II}Fe(C_2O_4)_3$ (M^{II} = Mn, Fe) give strong indications that the broadening observed in the observed profiles is a result of disorder arising from random faults in the stacking of the bimetallic *tris*-oxalate layers. In contrast the powder diffraction profiles of the corresponding $N(n\text{-}C_5H_{11})_4$ salts show that the microcrystalline samples are monophasic. Noting that $N(n\text{-}C_5H_{11})_4Fe^{II}Fe^{III}(C_2O_4)_3$ shows a large negative low field magnetization at low temperature, while the corresponding $N(n\text{-}C_3H_7)_4$ compound does not, we conjecture that it is the presence of interlayer disorder in the latter which prevents it, too, showing similar negative magnetization. It is noteworthy that the $P(C_6H_5)_4$ salt, which likewise shows no negative magnetization, likewise shows strong evidence for stacking faults in polycrystalline samples (14). Clearly the relation between interlayer

stacking disorder and bulk physical properties will need to be examined more closely in this class of material.

ACKNOWLEDGMENTS

We thank Dr. M. A. Green for helpful discussions. This work was supported by the UK Engineering and Physical Sciences Research Council.

REFERENCES

1. S. Decurtins, H. W. Schmalle, H. R. Oswald, A. Linden, J. Ensling, and P. Gutlich, and A. Hauser, *Inorg. Chim. Acta* **216**(1), 65 (1994).
2. C. Mathoniere, C. J. Nuttall, S. G. Carling, and P. Day, *Inorg. Chem.* **35,** 1201 (1996).
3. H. Tamaki, Z. J. Zhong, N. Matsumoto, S. Kida, M. Koikawa, N. Achiwa, Y. Hashimoto, and H. Ookawa, *J. Am. Chem. Soc.* **114,** 697 (1992); H. Tamaki, M. Mitsumi, K. Nakamura, N. Matsumoto, S. Kida, H. Ookawa, and S. Iijima, *Chem. Lett*., 1975 (1992).
4. M. Clemante-Leon, E. Coronado, J. R. Galan-Mascaros, J. Gomez-Garcia, *J. Chem. Soc. Chem. Commun*., 1727 (1997).
5. C. Mathonière, S. G. Carling, D. Yusheng, and P. Day, *J. Chem. Soc. Chem. Commun*., 1551 (1994).
6. O. L. Atovymann, G. V. Shilov, R. N. Lyubovskaya, E. I. Zhilyaeva, N. S. Ovaneseyan, S. I. Pirumova, I. G. Gusakovskaya, and Y. G. L. Morozov, *JETP Lett*. **58,** 767 (1993).
7. S. G. Carling, C. Mathonière, P. Day, K. M. A. Malik, S. J. Coles, and M. B. Hursthouse, *J. Chem. Soc. Dalton Trans*., 1839 (1996).
8. S. Decurtins, H.W. Schmalle, R. Pellaux, P. Schneuwly, and A. Hauser, *Inorg. Chem.* **35**, 1451 (1996).
9. J. Rodriguez-Carvajal, "FullProf—Short Reference Guide to the Program," 3.2 ed. Paris CEA-CNRS (1997).
10. B. E. Warren, *Phys. Rev.* **59,** 693 (1941).
11. M. M. J. Treacy, J. M. Newsham, and M. W. Deem, *Proc. Roy. Soc. London A* **433,** 499 (1991).
12. M. M. J. Treacy, "DIFFaX v1.766 (The Manual)," 1991.
13. The Molecular Simulations Incorporated MSI) software suite Insight II, with modules Solids Builder and Solids Adjuster was used to define the *P*1 layer. DIFFaX is provided as freeware with the MSI Catalysis suite.
14. C. J. Nuttall and P. Day, *Inorg. Chem.* **37,** 3885 (1998).